We are IntechOpen, the world's leading publisher of Open Access books Built by scientists, for scientists

4,800
Open access books available

122,000
International authors and editors

135M
Downloads

Our authors are among the

154
Countries delivered to

TOP 1%
most cited scientists

12.2%
Contributors from top 500 universities

CLARIVATE ANALYTICS BOOK CITATION INDEX INDEXED

WEB OF SCIENCE™

Selection of our books indexed in the Book Citation Index in Web of Science™ Core Collection (BKCI)

Interested in publishing with us?
Contact book.department@intechopen.com

Numbers displayed above are based on latest data collected.
For more information visit www.intechopen.com

Chapter 4

TiO_2 Nanostructures and Nanocomposites for Sustainable Photocatalytic Water Purification

Giuseppe Cacciato, Massimo Zimbone,
Francesco Ruffino and Maria Grazia Grimaldi

Additional information is available at the end of the chapter

http://dx.doi.org/10.5772/62620

Abstract

Water, together with energy and food, has been addressed as one of the main urgent problems of humanity. The conventional wastewater treatments suffer some limitations related to the effectiveness in decontamination (mechanical filtration), in the heavy use of chemicals (chlorination), or in elevation of operational costs and energy requirements (desalination and reverse osmosis). In this sense, new materials such as nanocomposites may overcome these issues taking advantage of the peculiar properties of materials at nanoscale. Research on novel nanotechnologies must bring advances in order to contrast and prevent water scarcity and pollution. In order to be effective, these nanotechnologies should run at low operational cost, even in places unequipped by strong infrastructures and in concert with conventional cheap methodologies.

Among the alternative water purification methods, TiO_2-based photocatalysis has attracted great attention due to material stability, abundance, non-toxicity and high decontamination efficiency. In this material, electron–hole pairs generated by light absorption separate from each other and migrate to catalytically active sites at the surface of the photocatalyst. Photogenerated carriers are able to induce the decomposition of organic pollutants as well as the deactivation of bacteria and viruses. The main deficiency of this material, related to its large bandgap, is that only the UV fraction of the solar spectrum which is effective to this purpose. Several approaches have been proposed to overpass this issue and, among them, the use of metal–TiO_2 nanocomposites with proper nanostructuration seems very promising for water purification strategies.

Keywords: TiO_2, photocatalysis, water purification, nanocomposites, plasmonics

1. Introduction

Among the alternative water purification methods, TiO_2-based photocatalysis has attracted great attention due to material stability, abundance, non-toxicity and high activity [1–3]. In this material, electron–hole pairs generated by a flux of photons, separated from each other and migrated to catalytically active sites at the surface of the photocatalyst. Photogenerated carriers are able to induce the water-splitting reaction and to decompose organic pollutants. Depending on the reaction path, highly reactive species (OH •,O_2^-,H_2O_2) can be created in solution. These reactants are able to decompose and mineralize most of the organic pollutants in solution as well as destroy bacteria [2]. The main deficiency of titanium dioxide relies on its wide bandgap (~3.2 eV) that makes it inefficient for solar-driven applications. However, proper nanostructuration of titanium dioxide and metal–TiO_2 nanocomposites have been demonstrated which is able to improve its efficiency, thus making this material an ideal candidate for water purification strategies.

Photocatalytic reactions are always the result of complex and concurring processes occurring on the surface at the nanoscale [2, 4]: (i) the absorption of light creating electron–hole excitations in a thin layer of a semiconducting compound, (ii) the separation followed by (iii) the transfer of these charges to the surface in contact with water or air, (iv) their interaction with organic or inorganic molecules located on this surface through oxidation and reduction reactions, leading finally (v), the electronic semiconductor system to recover its ground state. These processes are sketched in **Figure 1**. In this figure, an energetic photon generates a e^-/h^+ pair. The carriers can recombine at a surface trap (A) or in the bulk (B); otherwise, they can interact with acceptor (C) or donor (D) species adsorbed on the surface.

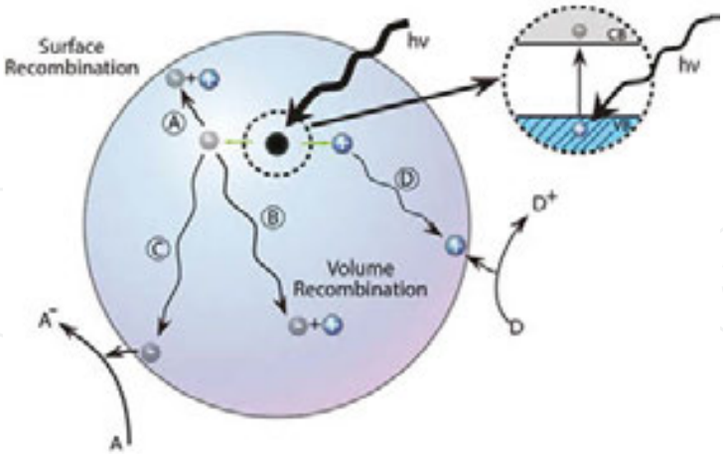

Figure 1. Schematic representation of the phenomena taking place in a semiconductor photocatalyst. The photogenerated carriers can recombine at a surface trap (A) or in the bulk (B); otherwise, they can interact with acceptor (C) or donor (D) species. Adapted with permission from Linsebigler et al. [5]. Copyright ©1995, American Chemical Society.

In **Figure 2** are reported the valence band (VB) and the conduction band (CB) positions (at pH = 0) for a range of semiconductors on a potential scale (V) versus the normal hydrogen electrode (NHE). As an example of the reactions taking place on the surface of the semiconductor, we

http://dx.doi.org/10.5772/62620

analyse more in depth the case of the water splitting. Dashed red lines in **Figure 2** represent the energy levels for the water-splitting half-reactions. For the water-splitting reaction to be thermodynamically favourable, the bandgap of the semiconductor photocatalyst should straddle these redox potentials, that is, the CB should have higher energy (more negative potential) than the hydrogen-evolution potential and the VB should be lower in energy (more positive potential) than the oxygen-evolution potential. So electrons can lower their energy being transferred to H^+ in solution and holes lower their energy being transferred to H_2O molecules through a short-circuited reaction and balancing the charges transferred to the solution. The final results are H_2 and O_2 molecules.

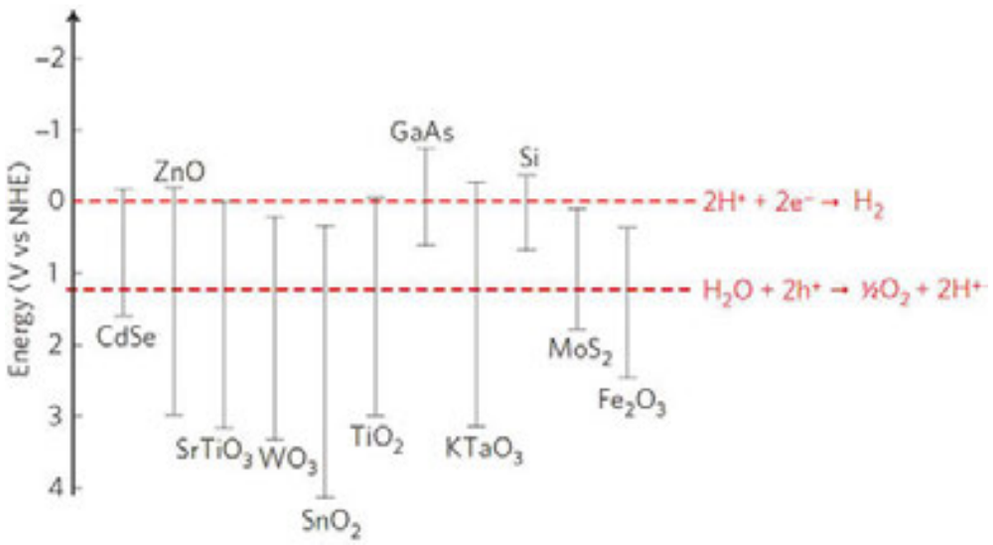

Figure 2. VB and CB for a range of semiconductors on a potential scale (V) versus the normal hydrogen electrode (NHE) at pH = 0. Redox potentials for the water-splitting half-reactions versus the NHE are also indicated by dashed red lines. Reprinted with permission from Linic et al [6]. Copyright ©2011, Macmillan Publisher Ltd.

Prior to the Honda–Fujishima effect in titanium dioxide [7], the interest in photocatalysis was centred on ZnO, which has similar CB and VB to TiO_2. The material is, however, limited by intrinsic photocorrosion upon excitation in aqueous media by the photoinduced hole weakening of Zn^{2+}–O^{2-} bonds to produce O_2 and soluble Zn^{2+} [8]. Hematite (α-Fe_2O_3) is another material that was originally thought to be an ideal photocatalyst due to its low cost, abundance and narrow bandgap for harnessing solar energy (bandgap = 2.0–2.2 eV, excitation wavelength up to 620 nm) [9]. However, the material suffers from rapid charge recombination (lifetime <10 ps) and a short charge carrier diffusion length (2–4 nm) [9]. Tungsten trioxide (WO_3) is another narrow bandgap material (bandgap = 2.7 eV) that has received fresh interest. The primary disadvantage of WO_3 lies in its low CB, which is below that required for the single-electron reduction of molecular oxygen [9]. Despite the narrow bandgap and the ideal position of VB and CB energy levels with respect to water-splitting semi-reactions potentials, CdSe (either in bulk or in quantum dot) is known to be toxic [10], thus is not suitable for pollution remediation in water.

The interest in titanium dioxide as the most studied photocatalytic material remains indisputable. This material has the advantage of being stable, abundant, non-toxic and highly active [1–3]. TiO_2 has three main polymorphs [11]: rutile (stable), anatase (metastable) and brookite (metastable). These have diverse activities for photocatalytic reactions, but the precise reasons for differing activities are a matter of debate and have not still been elucidated in detail. The most common studied phases are anatase and rutile. The commercial standard is the Aeroxide P25® (formerly Degussa P25). The P25 is a powder composed by a mixture of anatase (75%) and rutile (25%) [12]. There is a large debate in the literature claiming whether rutile or anatase is the best phase for photocatalytic reaction. Anatase seems to be more active than rutile [13], even if some studies suggest that the mixture of the two phases is the best compromise [14]. Moreover, one has to consider that, in view of decontamination strategies, the use of a photocatalyst fixed onto a substrate instead of a powder dispersed in solution may represent a clear advantage.

2. TiO_2-based photocatalysis

Photocatalysis is generally thought of as the catalysis of a chemical reaction induced by light at a solid surface. This implies that there must be at least two reactions occurring simultaneously, the first involving oxidation, from photogenerated holes, and the second involving reduction, from photogenerated electrons. Both processes must be balanced precisely in order to conserve the charge neutrality and for the photocatalyst itself not to undergo change (which is one of the basic requirements for a catalyst). In other words, photocatalysis is based on short-circuited photoelectrochemical reactions, balancing electrons and holes [2]:

$$h\upsilon \rightarrow e^- + h^+ \tag{1}$$

$$2H_2O + 4h^+ \rightarrow O_2 + 4H^+ \tag{2}$$

$$O_2 + 4H^+ + 4e^- \rightarrow 2H_2O \tag{3}$$

Because reduction or oxidation by the photoinduced charges of the reacting species involves electron transfer, these redox processes usually occur with species adsorbed to the surface. In competition with the charge carriers transfer processes, recombination takes place, either in bulk or at the surface. Retarding the recombination processes could effectively enhance the photocatalytic activity. Thereby, the presence of shallow trap centres at the surface could extend the mean lifetime of e^-/h^+ pairs. The typical timescale in photocatalytic reactions is reported in **Figure 3**.

http://dx.doi.org/10.5772/62620

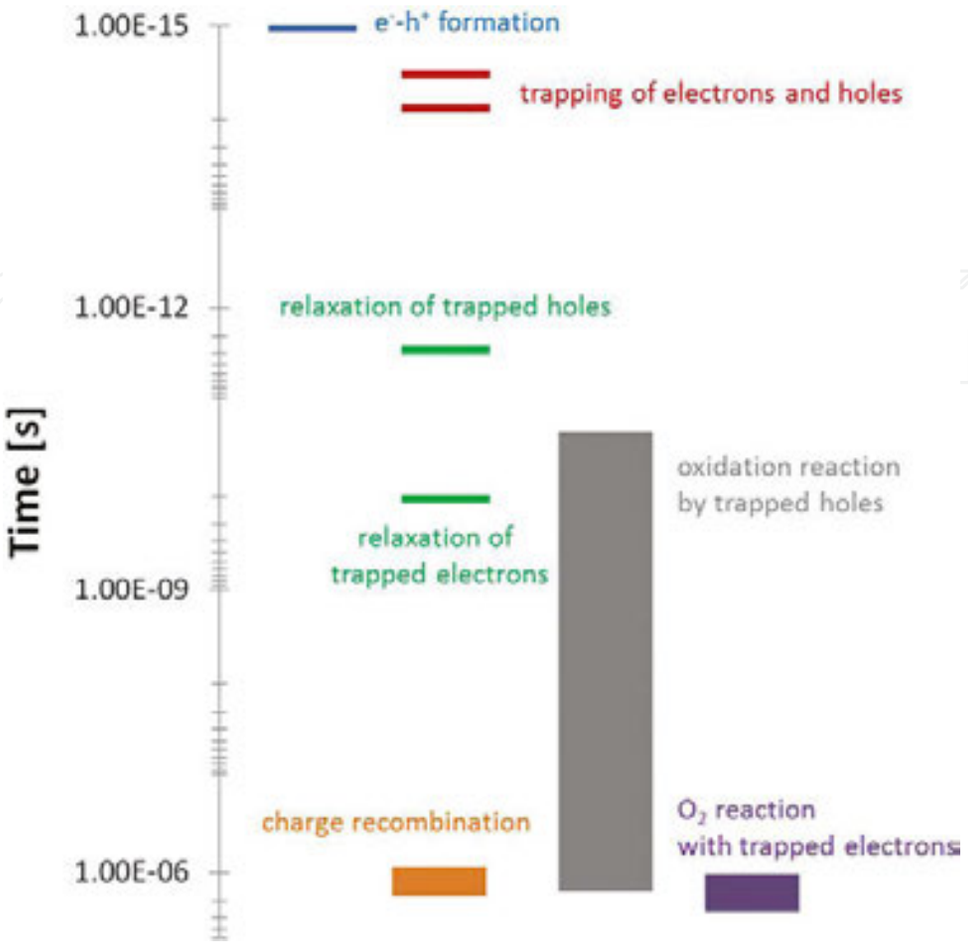

Figure 3. Time-scale in photocatalysis. Data taken 2008, Elsevier. with permission from Fujishima et al. [2].

Even in a perfect crystal, one observes the occurrence of a certain number of defects, especially at the surface. In particular, in TiO_2, the n-type behaviour is induced by the occurrence of oxygen vacancies [2]. In correspondence of these particular locations, there will be a trap centre for carriers, whose position in the band diagram will depend on the type of defect. Since h^+ are attracted by oxygen atoms in the lattice, while e^- are attracted by Ti^{4+}, one can state that defects which influence oxygen or titanium in the lattice correspond to level close to the VB or close to the CB, respectively. Actually, the most common defects in TiO_2 are represented by an oxygen vacancies and interstitial Ti [2]. The Ti^{4+} site left from this vacancy can attract an e^-, thus becoming a Ti^{3+} site. Non-coordinated Ti^{3+} on the surface is an ideal site for adsorption of oxygen [2]. Moreover, when two oxygen vacancies are close to the same Ti site on the surface, then the Ti atom can translate from its position, thus becoming an interstitial defect. Furthermore, interstitial Ti^{4+}, interacting with the oxygen of the TiO_2 lattice, is considered a trap for photogenerated holes [15].

In TiO_2 photocatalysis, surface adsorbed O_2 acts as the primary electron acceptor and no photocatalytic organic degradation is observed to occur in the absence of O_2 [4]. The reduction of O_2 has been demonstrated to be the rate-limiting step in semiconductor photocatalysis [4]. O_2 plays a critical role in enhancing photocatalysis by acting as an electron scavenger, thus

reducing e^-/h^+ pair recombination and forming highly oxidative species such as H_2O_2. These reactive oxygen species contribute to the oxidation of organic compounds by either directly attacking the organic or by producing hydrogen peroxide, which is a source of hydroxyl radicals that act as a strong oxidizer as shown in:

$$O_2 + 2e^- + 2H^+ \rightarrow H_2O_2 \rightarrow 2HO \quad (4)$$

In aqueous solutions, several different pathways have been suggested for O_2 reduction. For example, Hoffman suggested that O_2 first adsorbs to the TiO_2 surface before gaining an electron and then combines with two protons to form H_2O_2, which subsequently converts to hydroxyl species that degrade organic compounds [2, 4]. Nakamura proposed two mechanisms for this process; in the first one, an O^- on the TiO_2 surface transfers an electron to an O_2 in solution that then reacts with H^+ to form HO_2^- and eventually H_2O_2; in the second mechanism, an O_2 in solution adsorbs to a surface Ti^{4+} site by sequentially accepting two electrons and reacting with two protons to form H_2O_2 [16]. Similarly, Mattioli *et al.* suggested that O_2 accepts two electrons as it adsorbs on the TiO_2 surface and subsequently accepts two protons to form adsorbed H_2O_2, which then desorbs [17]. Surface adsorbed water or hydroxide anions act as the main hole acceptors in TiO_2 photocatalysis, although it has been suggested that certain organic materials may be directly oxidized by holes from TiO_2 [2, 4]. Indeed, holes are primary oxidizing species in photocatalytic reactions.

Most organic pollutant in water can be decomposed and mineralized on the surface of TiO_2 under UV irradiation. There are, obviously, several factors affecting the mineralization processes: light intensity, pH, ions dispersed in solution, etc. [2]. TiO_2 photocatalytic reactions reasonably follow first-order kinetics with respect to the concentration of the organic compound adsorbed, and α order with respect to light intensity [4]:

$$r = k\Gamma I^{\alpha} 5 \quad (5)$$

where r is the reaction rate, k the first-order constant, Γ the concentration of the organic compound for surface unity and I the light intensity. At high intensity $0 < \alpha < 1$, while at low intensity $\alpha = 1$.

Due to its wide bandgap, TiO_2 (either rutile or anatase) absorbs only in the UV range of the electromagnetic spectrum. However, sunlight contains a small amount of UV photons (~5%). Thus, in the last 20 years, several strategies have been developed, which devoted to increase the efficiency of titanium dioxide under visible (solar) irradiation. Among the most extensively studied methods, we cite the doping with N [18], transition metals [19] and C [20], the coupling with a narrow bandgap semiconductor quantum dots [21], the preparation of oxygen-deficient and/or hydrogen-rich TiO_x [22, 23] and the use of plasmonic metal nanostructures [6, 24]. We are interested, in particular, in these last two approaches.

http://dx.doi.org/10.5772/62620

3. Metal–TiO_2 nanocomposites

The typical response of a metal nanostructure excited by an electromagnetic wave is governed by the response of the electron gas in the metal. The simplest model describing the electron gas oscillations is similar to that of a damped harmonic oscillator. When matching the proper wavelength (frequency), it is possible to observe the so-called localized surface plasmon resonance (LSPR). LSPRs are non-propagating excitations of the conduction electrons of the nanoparticles (NPs). In the case of a spherical metal NP interacting with an incident electromagnetic wave, the response is determined by the particle polarizability [25]:

$$\alpha = 4\pi a^3 \frac{\varepsilon - \varepsilon_m}{\varepsilon + 2\varepsilon_m} \tag{6}$$

being a the particle radius, ε and ε_m the complex dielectric function of the metal and the embedding medium, respectively. The polarizability experiences a resonant enhancement under the condition that $|\varepsilon + 2\varepsilon_m|$ is a minimum, which for the case of small or slowly varying $\Im\{\varepsilon\}$ around the resonance simplifies to:

$$\Re\left\{\varepsilon(\omega)\right\} = -2\varepsilon_m \tag{7}$$

This relationship is called the Fröhlich condition and the associated mode (in an oscillating field) the *dipole surface plasmon* of the metal NP. In the quasi-static approximation ($a \ll \lambda$), a metal NP can be represented as an ideal dipole and spatial retardation effects over the particle volume can thus neglected. The scattering and absorption cross sections, calculated via the Poynting vector, are given by [25, 26]:

$$\sigma_{sca} = \frac{k^4}{6\pi}|\alpha|^2 = \frac{8\pi}{3}k^4 a^6 \left|\frac{\varepsilon - \varepsilon_m}{\varepsilon + 2\varepsilon_m}\right|^2 \tag{8}$$

$$\sigma_{abs} = k\Im\{\alpha\} = 4\pi k a^3 \Im\left\{\frac{\varepsilon - \varepsilon_m}{\varepsilon + 2\varepsilon_m}\right\} \tag{9}$$

where $k = \frac{2\pi}{\lambda}$ is the wavenumber.

For noble metals, silver and gold, in air the resonance is observed in the visible region of the electromagnetic spectrum. Indeed, the wavelength (energy) at which plasmon resonance occurs strongly depends on the metal. At a fixed electron density (i.e. for a certain metal), the plasmon resonance peak depends on the shape and on the dimension of the nanostructure [27–29].

In **Figure 4** the experimental data for Ag nanostructures having different shapes are shown. In general, it is not obvious to predict how a certain shape will influence the position of the resonance peak.

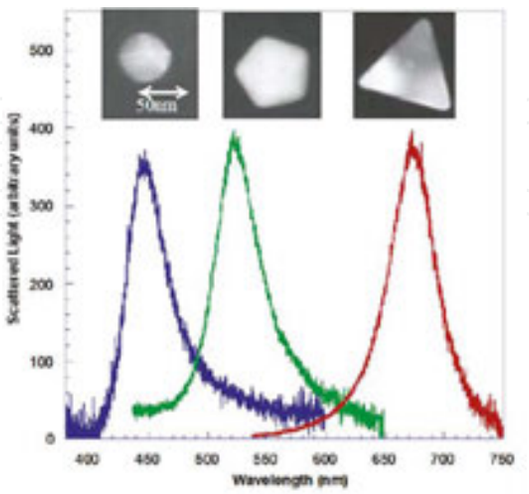

Figure 4. Experimental optical spectroscopy measurements of individual Silver nanoparticles having different shapes. Reprinted with permission from Mock et al. [28]. Copyright ©2002, AIP Publishing LLC.

However, asymmetric and complex shapes can reveal several resonances, depending on the polarization of incident light [27,30]. In **Figure 5** are reported the UV–Vis spectra of Ag nanoplatelets whose transversal size is fixed (20 nm), while the longitudinal length varies in the range between 65 and 92 nm [30]. These data are interesting since it is possible to observe two resonance peaks. The first one, located at about 400 nm, is fixed for all the samples and is related to the transversal size of the nanostructures. The second one red shifts from about 500 nm to about 650 nm and, at the same time, broaden as the longitudinal dimension increases.

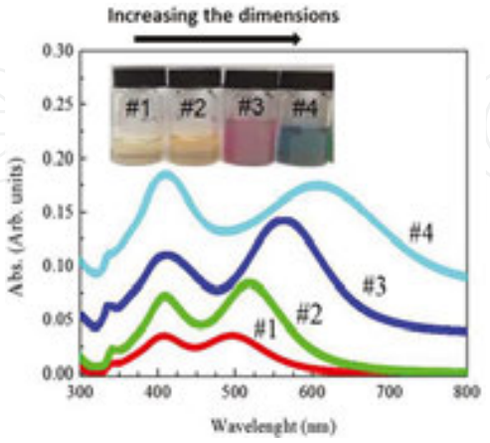

Figure 5. UV–Vis spectra of different Ag nanoplatelet solutions. The nanoplatelets have a transversal size of 20 nm and a longitudinal length in the range 65–92 nm (growing from sample #1 to sample #4). In the inset, a photograph of the corresponding solutions is shown. Reprinted with permission from Zimbone et al. [30]. Springer.

http://dx.doi.org/10.5772/62620

Two mechanisms occur as the nanostructure size increases: a red shift and a broadening of the resonance peak [31]. The first one is due to the *dynamic depolarization*: increasing particle dimensions, conduction electrons no longer move in phase, reducing the depolarization field and thus the restoring force, causing a red shift of the resonance. The second one is due to the *radiative damping*: as scattering becomes significant, this re-radiation leads to a radiative damping correction to the quasi-static polarizability and the effect of which is to significantly broaden the plasmon resonance.

The red shift and broadening of the resonance with increased NP size would generally be expected to be an advantage for solar-driven applications, since it translates in an enlarged absorption of the visible spectrum.

As already pointed out, the dielectric constant of the embedding medium also dramatically influences the plasmon resonance and its quality factor [27]. In **Figure 6** are reported the simulations of the extinction spectra of a silver sphere having diameter of 3 nm immersed in air (refractive index $n = 1$), glass ($n = 1.4$) or TiO_2 ($n = 2.7$). The simulations clearly show how the plasmon peak shifts to higher wavelengths (lower energies) as the refractive index increases. At the same time, one observes an increase of the quality factor of the resonance, due to a higher confinement of the electric field.

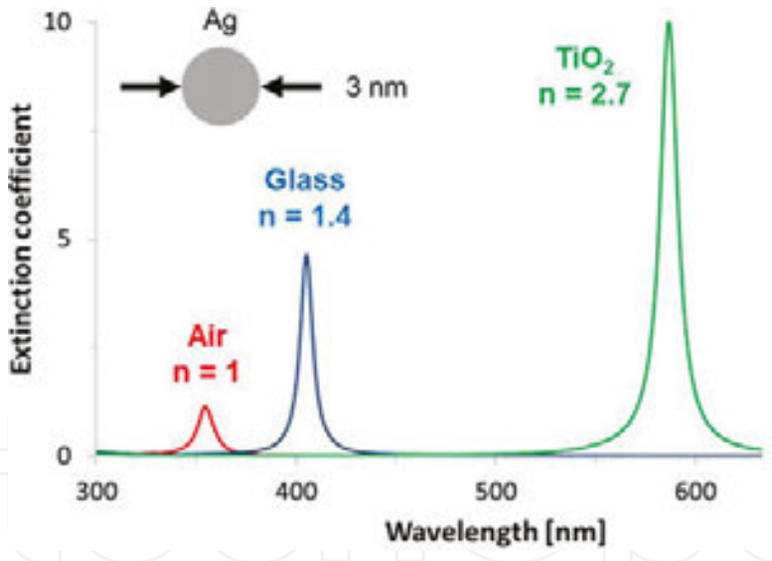

Figure 6. Simulation of the extinction spectra versus wavelength of a silver sphere having diameter of 3 nm immersed in air (red), glass (blue) or TiO_2 (green). The refractive index (at the resonance peak wavelength) of each medium is also reported.

As previously mentioned, in the neighbouring of the plasmonic metal, NP one observes a high enhancement of the electromagnetic field, in particular during the occurrence of a LSPR. Such a high rise in the intensity of the field can, in principle, lead to nonlinear effects both in the metal particle and in the embedding matrix. In **Figure 7** is reported the simulated magnitude of the electromagnetic field in the vicinity of a silver nanocube of diameter 75 nm, at a wavelength of $\lambda = 420$ nm matching the plasmon resonance [6]. The field intensity is redis-

tributed leading to a region where the field enhancement reaches a factor up to 10^3 times the incident intensity.

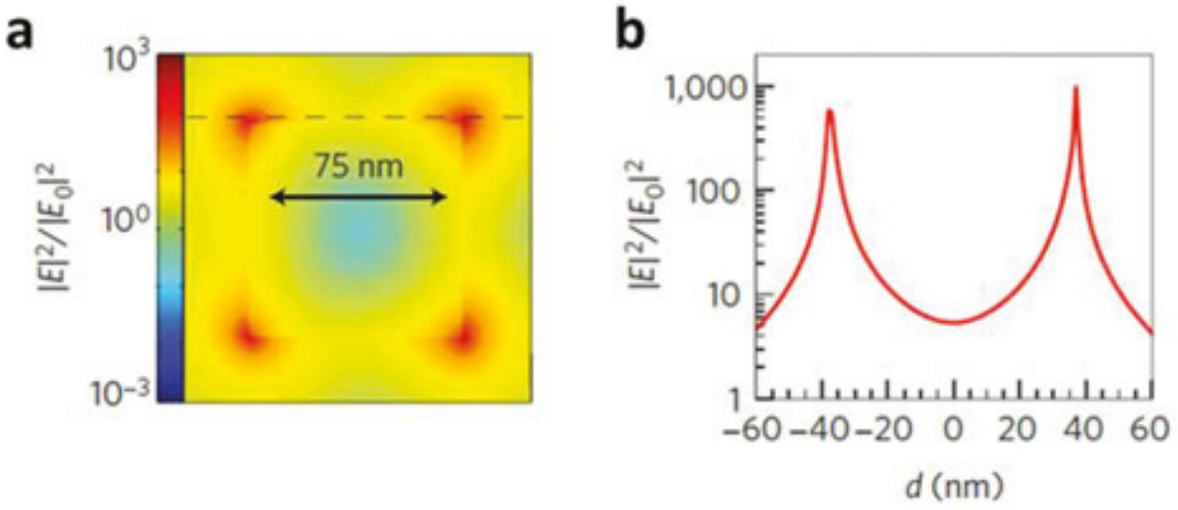

Figure 7. (a) Spatial distribution of the LSPR-induced enhancement of electric field intensity at the LSPR peak wavelength (420 nm), from a finite-difference time-domain (FDTD) simulation of a 75-nm Ag nanocube. (b) Enhancement in the electric field intensity at the LSPR peak wavelength as a function of distance *d* along the dashed line indicated in (a). Reprinted with permission from Linic et al [6]. Copyright ©2011, Macmillan Publisher Ltd.

The field enhancement is particularly strong (up to a factor 10^4 with respect to the exciting electromagnetic field) inside metal gaps, that is in the space between two metal nanostructures close (few nm) each other [32, 33].

As previously mentioned, one of the main deficiencies of TiO_2 relies on its wide bandgap. In order to enhance the material efficiency in the visible range of the electromagnetic spectrum, surface-plasmon-mediated photocatalytic activity of TiO_2 has become a hot research topic [6, 24, 34–40].

As depicted in **Figure 8**, metal nanostructures in the presence of an external exciting electromagnetic field can interact with a photoactive substrate at least in three different ways [41]:

1. the far-field component of the scattered field will induce a prolonged optical path for photons and thereby will increase the probability of absorption within the semiconductor substrate;

2. the near-field component of the field can cause an enhancement of the field intensity in the vicinity of the nanostructure, thus leading to nonlinear effects as well as local heating effects;

3. as a consequence of the metal–semiconductor junction, a direct injection of photoexcited carriers into the substrate can occur as well as a charge separation process due to the Schottky barrier.

http://dx.doi.org/10.5772/62620

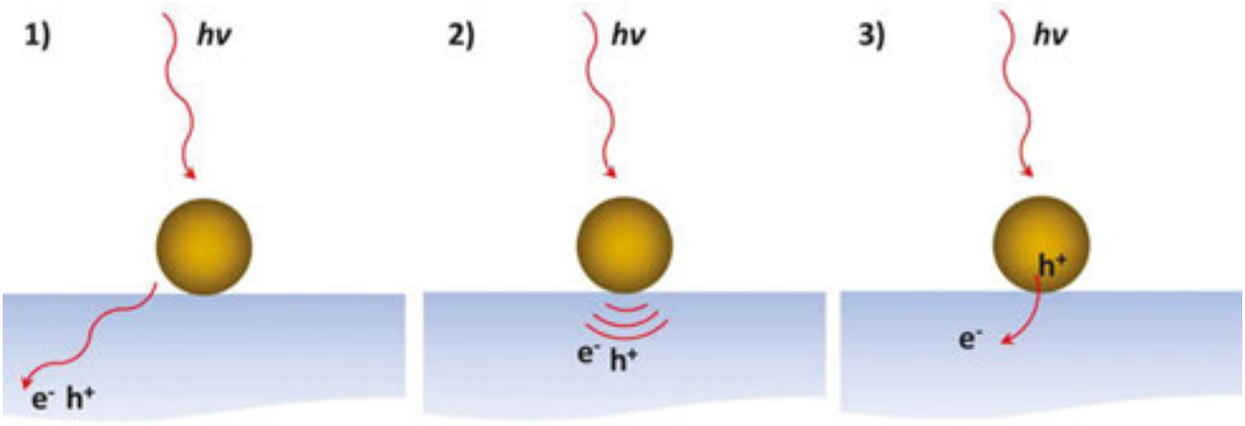

Figure 8. Schematic of different interactions between a metal nanoparticle and a photoactive substrate: (1) far-field scattering, (2) near-field scattering and (3) direct injection of photoexcited carriers into the semiconductor.

For photocatalysis, the last two effects are particularly important. The advantage of the formation of e^-/h^+ pairs, close to the semiconductor surface, is that these charge carriers are readily separated from each other and easily migrate to the surface, where they can perform photocatalytic transformations.

Experimental evidences of the improvement in the photocatalytic activity under visible irradiation have been recently reported [6, 24, 34, 42, 43]. In **Figure 9** is reported the comparison between oxygen and hydrogen evolution from solution of Ag–TiO_2 and bare TiO_2 nanocomposites upon illumination with a broadband visible source (400–900 nm, ~500 mW/cm^2, spectral peak at 580 nm) [42]. The solution was prepared mixing a colloidal solution of Ag nanocubes with nitrogen-doped TiO_2 (N–TiO_2) solution. The composite was 5% metal by weight.

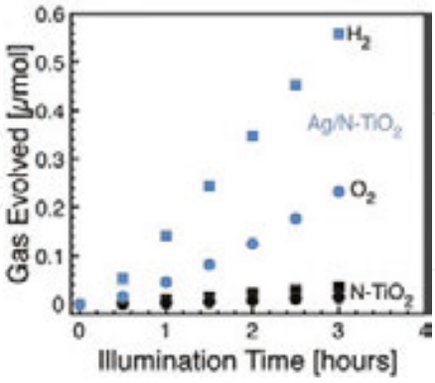

Figure 9. H_2 (squares) and O_2 (circles) production upon visible illumination of N–TiO_2 (black symbols) and Ag/N–TiO_2 (blue symbols) photocatalysts, as measured by mass spectrometry. Reprinted with permission from Ingram and Linic [42]. Copyright ©2011, American Chemical Society.

The presence of silver nanostructures is responsible for the enhancement in the activity of the photocatalyst through charge injection. According to this model, electrons near the metal Fermi

level E_f are excited to surface-plasmon (SP) states; then, after the relaxation of the plasmon oscillations, some electron can transfer to the nearby semiconductor and, at this point, activate electron-driven processes such as the hydrogen-evolution half-reaction [6, 44] (**Figure 10**).

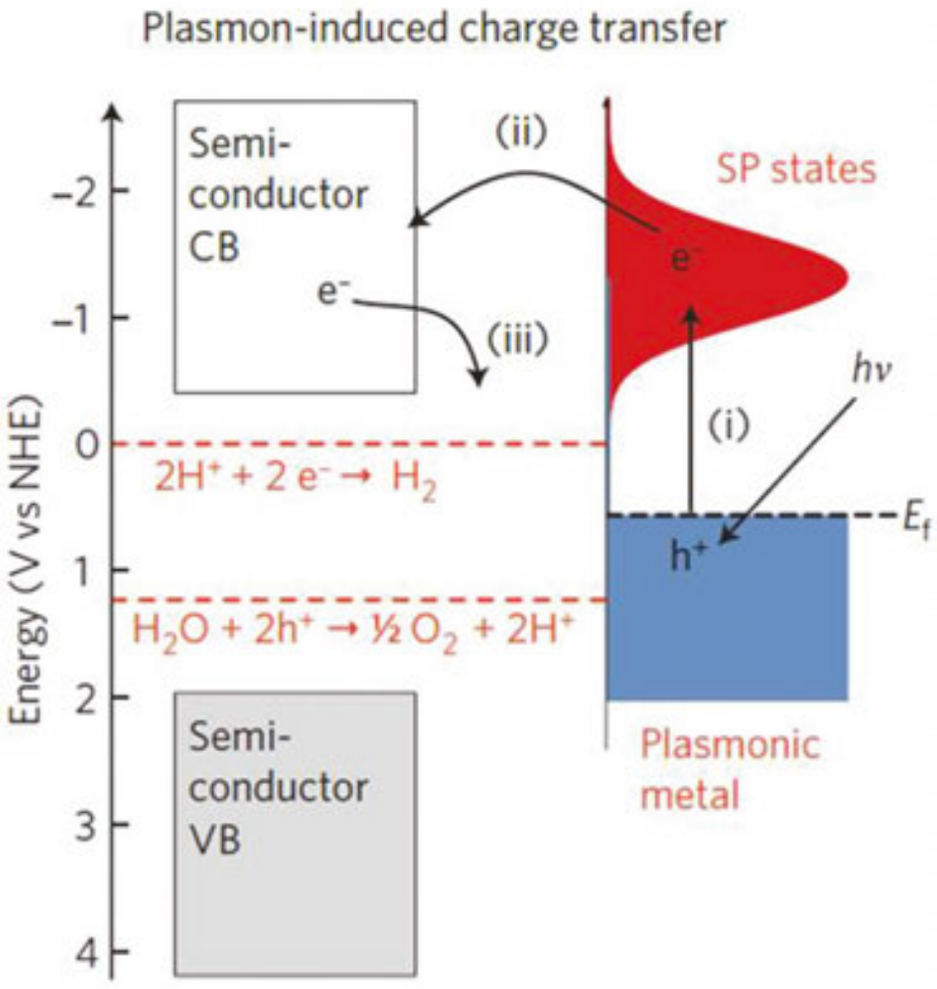

Figure 10. Mechanism of LSPR-induced charge transfer with approximate energy levels on the NHE scale. Dashed red lines refer to the water-splitting redox potentials (see **Figure 2**). Reprinted with permission from Linic et al [6]. Copyright ©2011, Macmillan Publisher Ltd.

In another experiment conducted by Liu et al. [43], the enhancement in the photoactivity of an Au–TiO_2 nanocomposite film is explained in terms of the local electric field enhancement near the TiO_2 surface, rather than by the direct transfer of charge between the two materials. According to the authors, in this case, the near-field optical enhancement increases the electron–hole pair generation rate at the surface of the TiO_2. In **Figure 11a–d** are reported the finite-difference time-domain (FDTD) simulations on a 5-nm thick Au film onto TiO_2 substrate, showing the presence and distribution of region of high electromagnetic field intensity (*hot spots*) within metal gaps. In **Figure 11e, f** are reported the experimental photocurrent measurements emphasizing the better performance of the Au–TiO_2 composite film in the spectral range of interest for LSPR in gold (red region of the visible spectra).

http://dx.doi.org/10.5772/62620

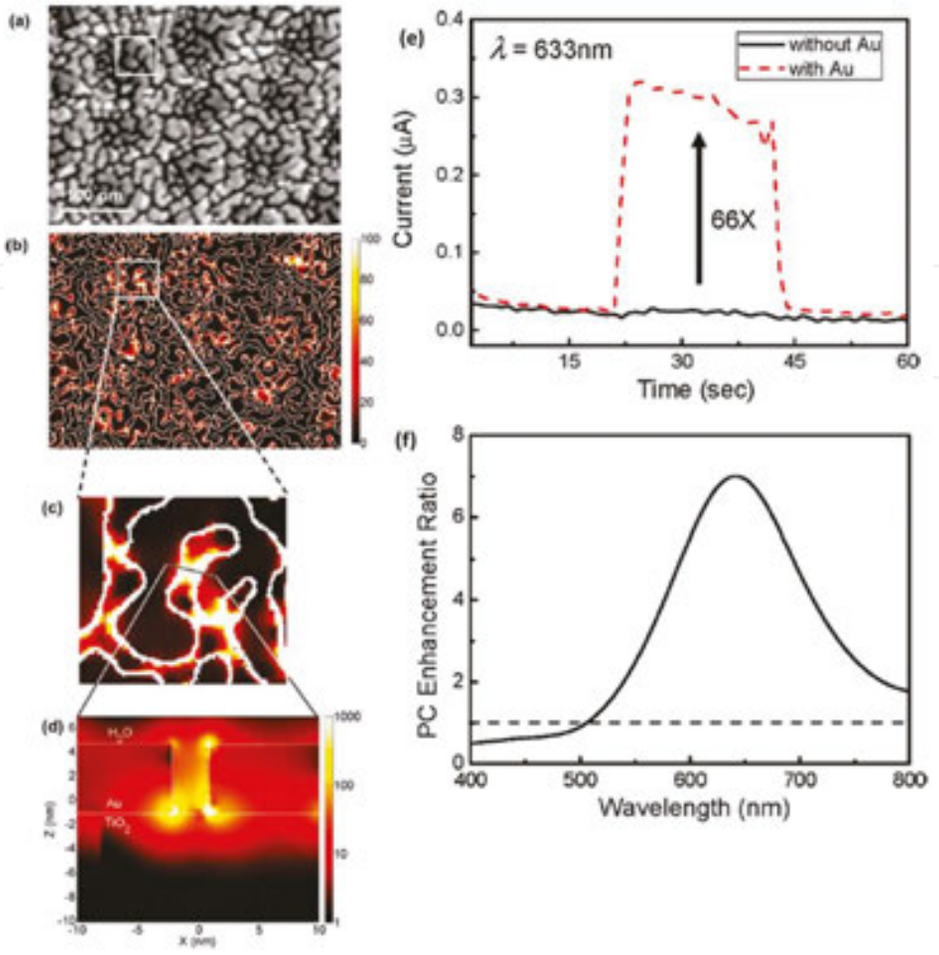

Figure 11. On the left, (a) SEM image of a 5-nm thick Au island film on TiO_2; FDTD-simulated electric field intensity, in the plane xy (b, c) and in a vertical section (d). On the right, (e) photocurrent of anodic TiO_2 with and without Au nanoparticles irradiated with λ = 633 nm light for 22 s; (f) photocurrent enhancement ratio spectrum; the dashed line refers to the bare TiO_2 (value 1). Reprinted with permission from Liu et al. [43]. Copyright ©2011, American Chemical Society.

However, it has been also proposed a photocatalytic reaction directly on the surface of the plasmon-excited metal NP [37, 44, 45]. In this picture, excited NP inject hot electrons to the states (orbitals) of the adsorbed species (reactants). It is a process similar to charge injection but without the mediation of the semiconductor material.

Whatever the process involved, it seems clear that the presence of metal nanostructures can effectively improve the efficiency under visible (solar) irradiation.

4. Optical engineering of Ag/TiO_2 nanocomposite films

4.1. Field enhancement engineering

In order to introduce the concept of field enhancement, let us consider a perfect mirror with a film of refractive index n grown on its surface. Let us consider a monochromatic wave in

normal incidence on this film. It is well known that an electromagnetic wave, passing through a film and being reflected backward, will undergo to a phase shift δ:

$$\delta = \frac{2\pi t}{\lambda_n} \tag{10}$$

where t is the film thickness and λ_n the wavelength in the medium. When measuring the reflectivity of a thin film on substrate, we obtain constructive interference for $2\delta = 2\pi m$, destructive interference for $2\delta = (2m + 1)\pi$, being m an integer. Thus, the thicknesses at which destructive or constructive interference occur are given by:

$$t = \frac{m\lambda_n}{2} \tag{11}$$

$$t = \frac{(2m+1)\lambda_n}{4} \tag{12}$$

It is worth noting that in destructive interference conditions, the electromagnetic field intensity at the air–film interface is at maximum. Indeed, in stationary state, thus considering the incident and reflected beam, we observe a node at the (perfect) mirror–dielectric interface; if we look at the intensity of the electromagnetic field ($\propto E^2$) versus the distance from the mirror, we can observe a maximum of the intensity of field at:

$$d = \frac{(2m+1)\lambda_n}{4} \tag{13}$$

Note how this distance equals the condition in Eq. (12), stating the antireflectivity conditions (i.e. destructive interference).

In **Figure 12** are shown the calculation made by Bayle et al. [46] in the case of a SiO_2/Si substrate. In this case, the wavelength in vacuum is chosen at 413 nm (in coincidence with the plasmon frequency of Ag NPs in SiO_2), the thickness of the layer is 210 nm (matching the antireflectivity conditions for the chosen wavelength), the incidence is normal. Firstly, one observes that, under these antireflectivity conditions, the intensity of the total electromagnetic field reaches the maximum at the air/SiO_2 interface. Indeed, in **Figure 12a**, the total electromagnetic field (resulting from incident and reflected electromagnetic waves) shows a maximum at the free surface of the matrix: the film thickness matches the condition (**Figure 12**), that is equal to the result in Eq. (13). This means that the film is in antireflective conditions. In **Figure 12b, c**, a layer of Ag nanocrystals (NCs) (the particles diameter 5 nm and the amount of silver equals 5×10^{16} atoms/cm^2) is placed into the oxide matrix. As it is possible to observe from the total electromagnetic field intensity, the same layer of Ag NPs can show or not an enhanced optical

http://dx.doi.org/10.5772/62620

response depending on the position, respectively, at a minimum (**Figure 12b**) or at a maximum (**Figure 12c**) of the field.

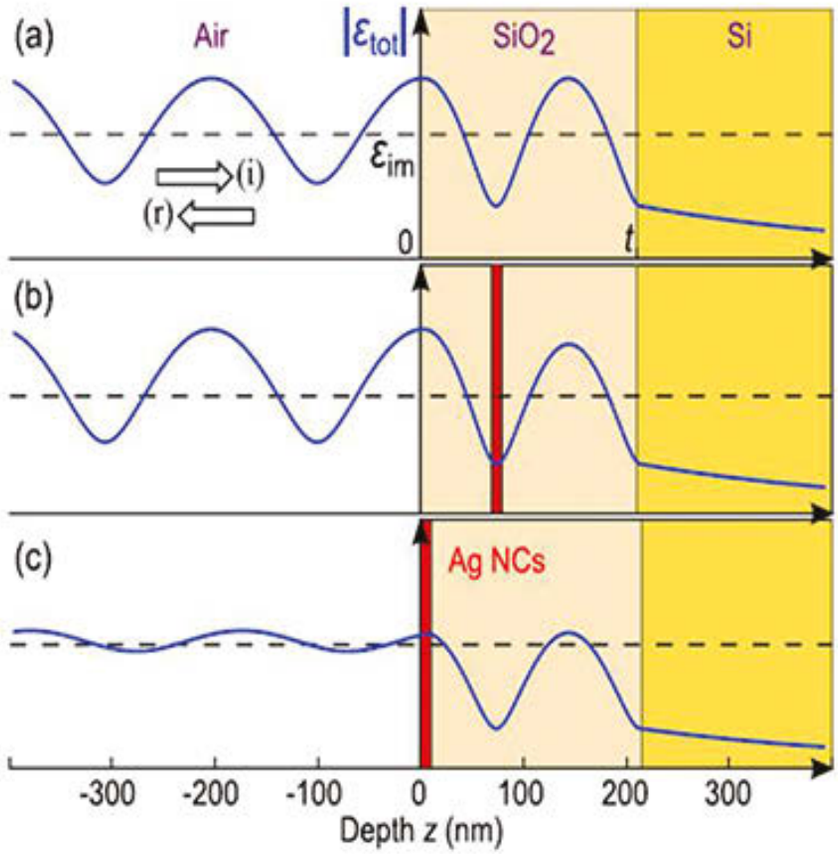

Figure 12. Variation versus depth of the amplitude of the total (incident *i* + reflected *r*) electric field $|E_{tot}|=|E_i + E_r|$: (a) without Ag NCs, (b) with a plane of Ag NCs located at a node of the electric field into the dielectric layer, and (c) with this plane located at an antinode of the electric field near the dielectric/air interface. Reprinted with permission from Bayle et al. [46]. Copyright ©2014, American Physical Society.

Therefore, engineering the architecture of the stacking layers is the key to take simultaneous advantage of spectrally and spatially LSPR but also of field enhancement. This has been recently proposed for enhanced spectroscopy and imaging by Carles et al. [47].

By choosing an appropriate thickness of a TiO_2 layer deposited on a silicon substrate, one can easily tune the spectral position of one of the antireflective minima in such a way it can match the LSPR. In particular, in **Figure 13b** is shown the extinction efficiency of a silver nanosphere (3 nm in diameter) embedded in air ($n = 1$), SiO_2 ($n \approx 1.4$) or TiO_2 ($n \approx 2.7$). We can observe how the LSPR red shifts and, at the same time, increases its quality factor as the refractive index of the embedding medium increases. This is due to the higher confinement of the electromagnetic field in high-refractive-index materials [26, 27]. In **Figure 13a** is shown the reflectance of a SiO_2 (or TiO_2)/Si heterostructure with embedded a Ag NPs layer. By choosing the proper film thickness, that is matching the antireflectivity conditions for the wavelength at which plasmon resonance occurs, it is possible to obtain an enhanced optical response from the NPs layer.

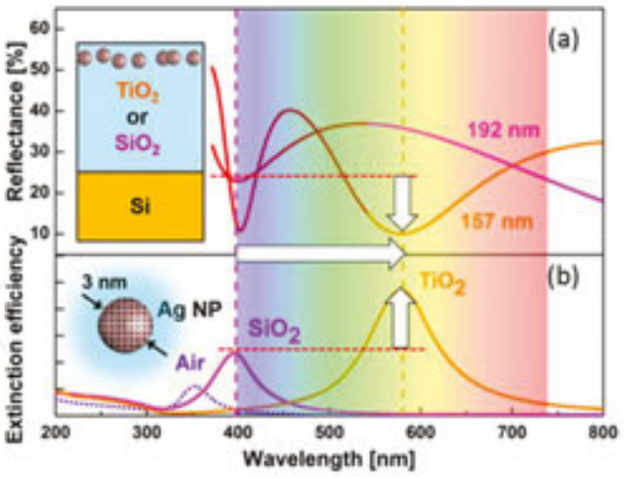

Figure 13. Theoretical simulation illustrating the tuning of anti-reflectivity condition in a TiO_2/Si heterostructure and LSPR in a silver nanoparticle of diameter D = 3 nm. Reproduced with permission from Cacciato et al. [40]. The Royal Society of Chemistry.

The aim of the work presented in this section was to take benefit of this phenomenon in multilayer stacking containing TiO_2 and embedding Ag NPs. They will be adapted to manage amplifying processes in the visible range by exploiting simultaneously the resulting optical interference phenomenon and LSPR.

4.2. TiO_2 subsurface embedded Ag NPs obtained via low energy ion beam synthesis

In our recent work [40], we demonstrated the importance of the optical engineering of the substrate supporting Ag NPs. Indeed, using low-energy ion implantation, we prepared a Ag/TiO_2 nanocomposite film showing a huge optical response when irradiated with a wavelength close to that of LSPR of Ag NPs. In **Figure 14**, a transmission electron microscopy (TEM) image of the as-implanted sample matching the field enhancement conditions is shown. A band of silver NPs 3 nm in diameter is evident few nm close to the free surface of the hosting TiO_2 matrix.

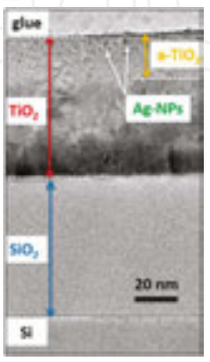

Figure 14. TEM cross-section image of Ag/TiO_2 sample, observed in bright field, showing the different stacked layers. Adapted with permission from Cacciato et al. [40]. The Royal Society of Chemistry.

http://dx.doi.org/10.5772/62620

More important, in this nanocomposite, the fingerprint of the charge injection from the NPs inside the TiO_2 matrix was revealed by means of Raman spectroscopy. In **Figure 15** are reported the Raman spectra of the Ag/TiO_2 samples under plasmon-resonant (532 nm) or out of resonance (638 nm) excitation. In order to demonstrate the importance of the optical engineering of the TiO_2 substrate, two different thicknesses were used, matching the field enhancement conditions (TiO_2 90 nm) or out of these conditions (TiO_2 165 nm). The spectra of the bare TiO_2 substrate are also reported for comparison. Focusing on the spectra in plasmon-resonant excitation, it is possible to observe the high enhancement in the response of the Ag/TiO_2 film matching the antireflective conditions (blue spectra). With respect to the bare TiO_2, which shows the characteristic peaks of rutile TiO_2 and Si, the Ag/TiO_2 spectra reveals the presence of new peaks. The peaks in the region below 200 cm^{-1} belongs to Ag phonons, as already observed in Ag nanocrystals in other dielectrics [46]. The bands at higher Raman shifts, between 650 and 900 cm^{-1}, are addressed to LO phonon–plasmon modes. This signal is absent out of resonance and without Ag NPs. These modes are due to the presence of free carriers injected in the TiO_2 matrix [40]. Similar electrons transfer from metallic NPs to a polar semiconductor is known in n- or p-doped semiconductors [48, 49] and high-Tc superconductors [50]. These modes have been also observed with IR reflectance spectroscopy in non-stoichiometric rutile [51] and anatase [52, 53].

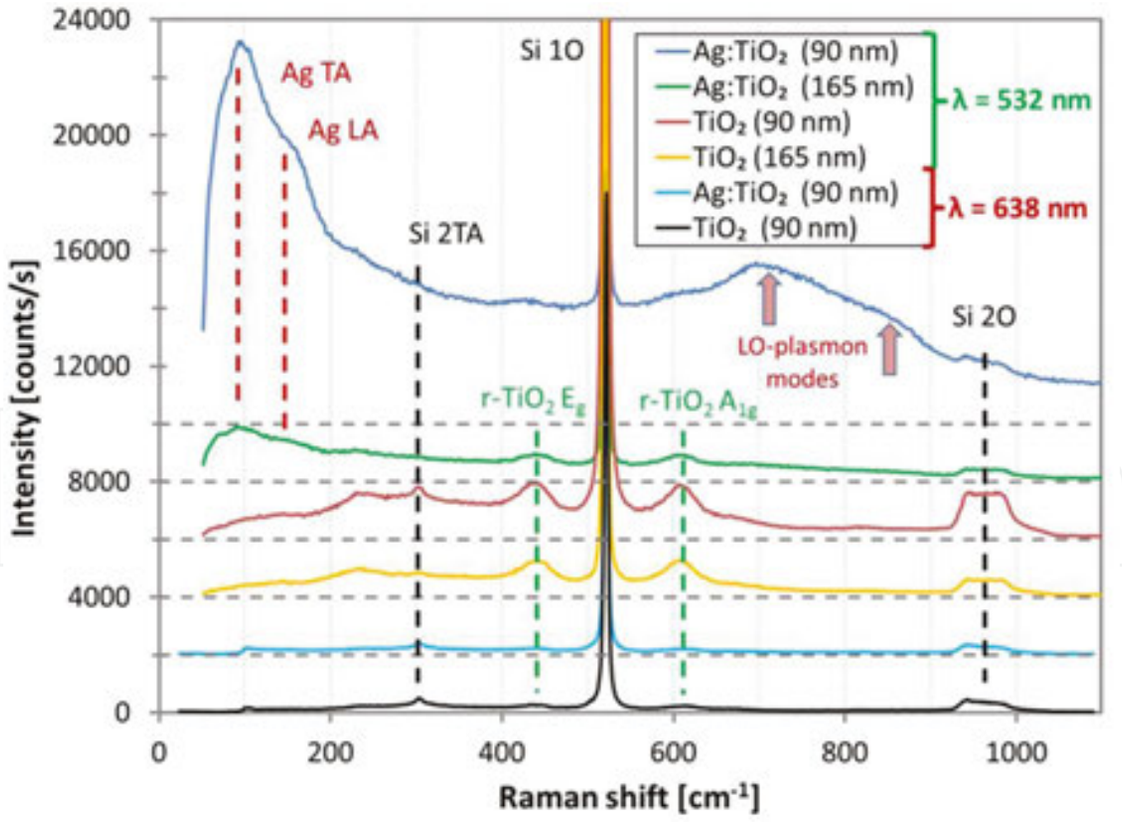

Figure 15. Raman spectra recorded on Ag/TiO_2 and bare TiO_2 of samples matching the field enhancement conditions (TiO_2 90 nm) or out of these conditions (TiO_2 165 nm) under plasmon-resonant excitation (532 nm) or out of resonance (638 nm). Reproduced with permission from Cacciato et al. [40]. The Royal Society of Chemistry.

Unfortunately, the photocatalytic tests did not show an activity enhancement induced by the implantation process and the presence of Ag NPs. On the contrary, a strong reduction was observed, probably due to charge carrier recombination on defects generated by the implantation process: the synthesis technique seems to damage irremediably the upper layer of the hosting TiO_2 matrix. Therefore, the consequent step should be to use a proper optically engineered substrate with embedded metal NPs through a technique that preserves the photoactive material. This will be the content of the next paragraph.

4.3. TiO_2/Ag/TiO_2 nanocomposite film obtained via sequential sputtering

The exposure of a photocatalytically active surface has been demonstrated of primary importance for the goal of efficient substrates for water purification [54]. At the same time, the optical engineering of the substrate can highly improve the response of the nanocomposite in the visible range, as reported in the previous paragraph. Therefore, the logical step towards solar-driven photocatalysis is to fabricate a TiO_2/AgNPs/TiO_2 multilayer using a technique that allows fine tuning of several parameters (particle size and position, thickness of each layer), while preserving the quality of the photoactive surface. For these reasons, we proposed sequential sputtering and annealing as methodology to elaborate a TiO_2/Ag/TiO_2 nanocomposite film [55]. In this case, the NPs synthesis occurs through the dewetting of the metal film. The dewetting is a process according to which the metal film deposited onto a substrate retracts under the action of the surface tension. The process is governed by the surface free energy of the metal, the substrate and the metal/substrate interface [56]. This mechanism is somehow similar to the formation of water droplets onto a hydrophobic surface. In **Figure 16** is shown a schematic representation of the steps followed to realize of the nanocomposite film: (a) realization of the TiO_2 'matrix' layer (realized for the antireflective propose), (b) deposition of the Ag film, (c) thermal annealing in order to realize the silver NPs through dewetting and (d) deposition of the TiO_2 protective layer.

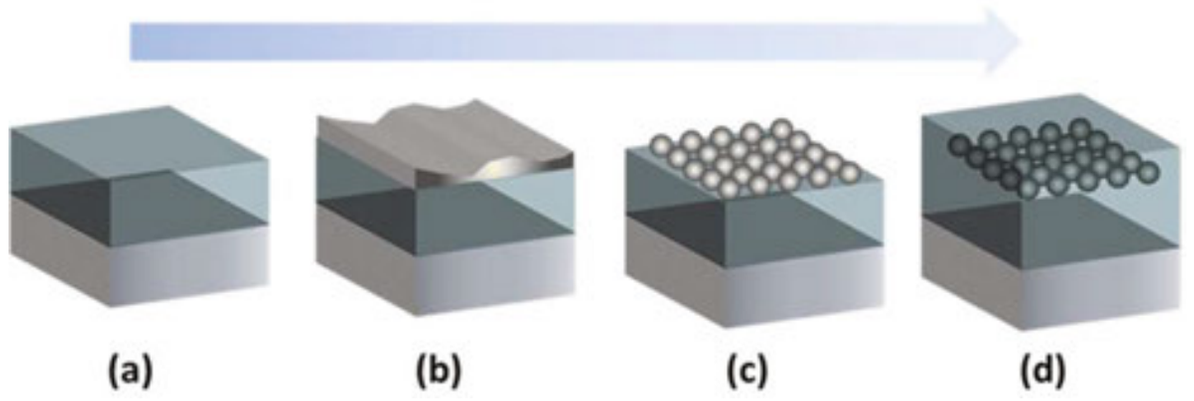

Figure 16. From left to right, schematic representation of the elaboration process: (a) TiO_2 substrate preparation, (b) Ag deposition, (c) nanostructuration via thermal annealing and (d) deposition of a TiO_2 capping layer.

A Ti film was grown by sputtering on Si <100> substrates. Polycrystalline (rutile) TiO_2 was obtained, starting from these substrates, by thermal oxidation at 600°C. Ag depositions on the

http://dx.doi.org/10.5772/62620

polycrystalline TiO_2 were carried out. A nominal thickness of d = 5 nm of Ag was deposited. After Ag depositions, samples were annealed in vacuum, at 400°C. The final 10 nm TiO_2 capping layer has been obtained via deposition of a thin Ti film followed by a thermal annealing at 400°C for 30 min in vacuum. Due to the low deposition rate, the deposited layer is already oxidized, so that the thermal annealing was required just to ensure the crystallinity of the capping layer. Anyway, this step has not influenced the underlying Ag nanostructured film.

Scanning electron microscopy (SEM) images in **Figure 17** clearly show the nanostructuration of the metal film (from **Figure 17b, c**) and then the conformal coverture of the final 10 nm thick TiO_2 layer (from **Figure 17c, d**).

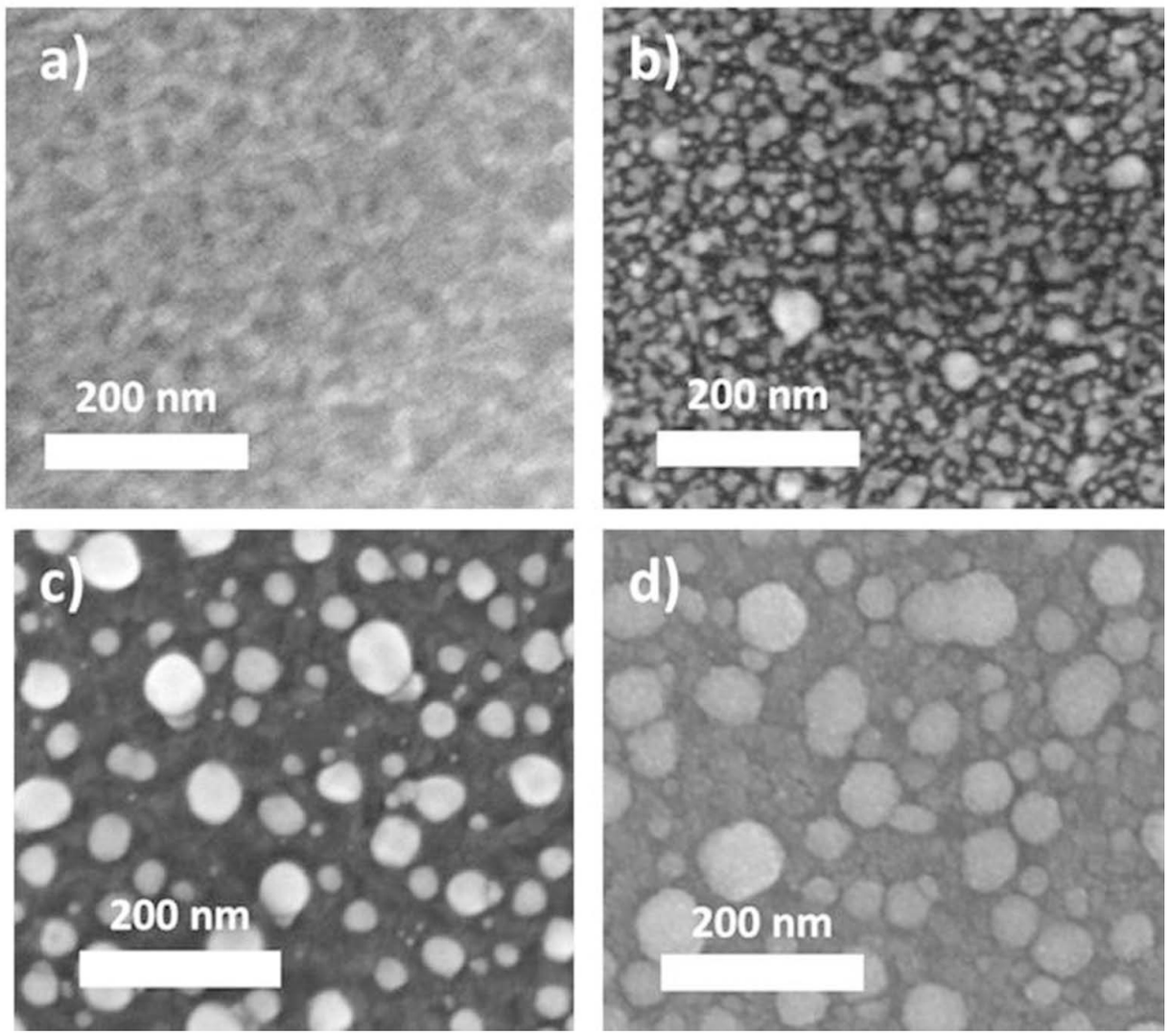

Figure 17. SEM images (plan view) of (a) the TiO_2 substrate, to (b) the Ag as deposited film, (c) the Ag/TiO_2 after annealing and finally, (d) the TiO_2 capping layer.

In order to have more insight on the photocatalysis, we tested the photoactivity of our samples by means of the discoloration of methylene blue (MB) dye. For the photocatalytic activity tests, we referred to the guidelines of the ISO 10678:2010 [57, 58]. The results of the test are summarized in **Figure 18**, where the discoloration rate normalized to the surface area is reported. We compared three samples: a TiO_2 10 nm/Ag NPs/TiO_2 190 nm nanocomposite in field enhancement conditions at the plasmon resonance wavelength of the obtained Ag NPs; a TiO_2 10 nm/Ag NPs/TiO_2 165 nm nanocomposite out of field enhancement conditions; a TiO_2 10 nm/TiO_2 165 nm whose last 10 nm where prepared in the same conditions as the capping layer of the Ag NPs of the nanocomposite samples. MB degradation occurs under irradiation; therefore, we reported also the degradation of a vessel not containing photocatalytic material as reference.

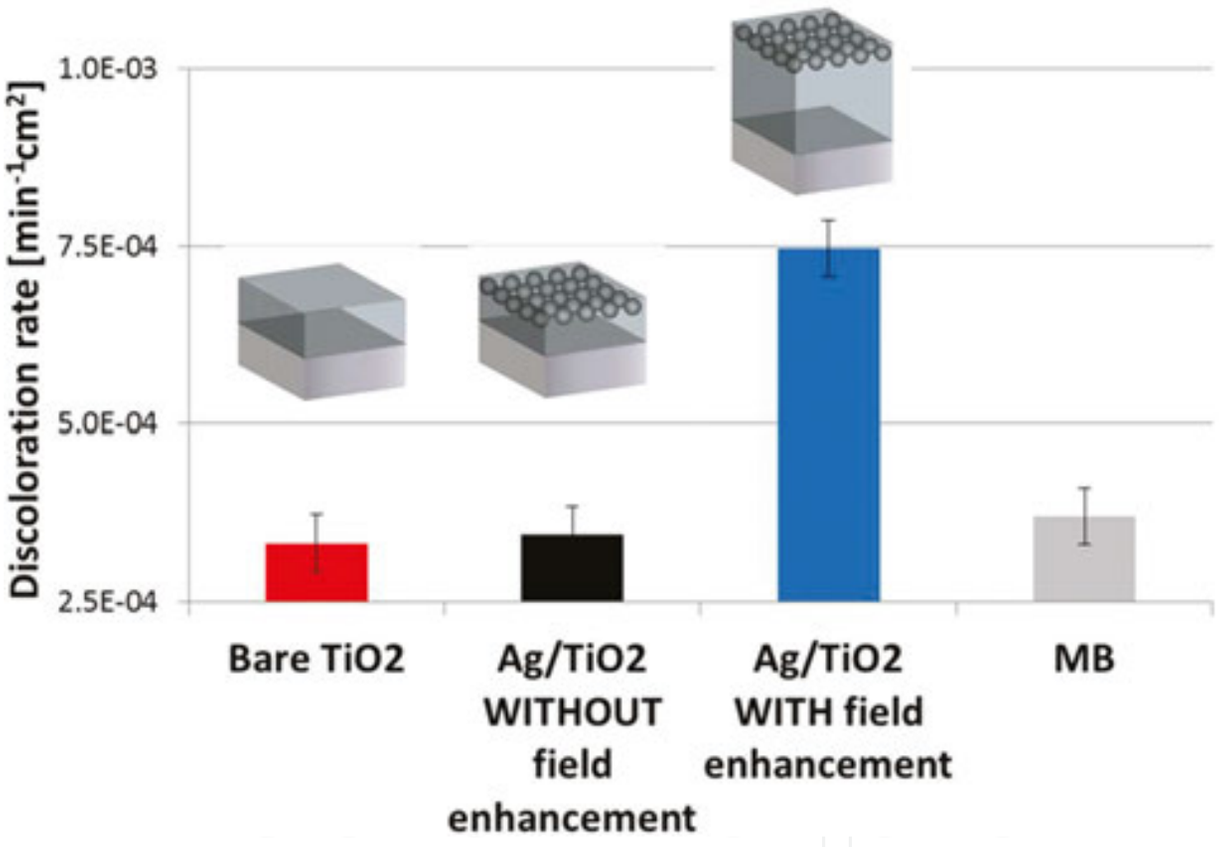

Figure 18. Discoloration test results under visible irradiation.

We observe that, as expected, TiO_2 is not active under visible illumination. The fundamental result of the test is that, despite having the same composition and superficial morphology, the two TiO_2/Ag/TiO_2 nanocomposite film show completely different behaviour. In particular, the film matching the antireflectivity conditions is able to decompose the MB dye, showing a good photocatalytic activity in the visible range, while the film outside these conditions appears to be not active. These results underline the importance of a proper optical engineering of the supporting matrix for plasmon enhanced applications.

http://dx.doi.org/10.5772/62620

4.4. Summary

We obtained an Ag/TiO_2 nanocomposite activated by visible irradiation. Such an activity, occurring at irradiation energies below the absorption threshold of titania (gap) and thus not observable in the bare TiO_2 film, has been ascribed to the presence of plasmonic metal NPs. Moreover, we observed a strong correlation between photocatalytic activity and field enhancement conditions. Therefore, we demonstrated the importance of proper film thickness engineering in order to take simultaneous advantage of plasmon resonances and optical interference. Actually, this result had been already demonstrated in [40], at least from the optical point of view. Such substrates are ideal candidates for solar-driven photocatalytic reactions. This result is actually more general and could be potentially employed in other plasmo-electronic applications (e.g. SERS,…).

5. Amorphous hydrogenated TiO_2 NPs

The second approach we want to suggest is based on the use of TiO_2 NPs. On the one hand, using NPs, the exposed surface increases of order of magnitude with respect to a photocatalytic film; on the other hand, issues related to the dispersion of the nanomaterial in the environment or to the recovery of the particles from the solution may arise.

Titanium oxides NPs can be obtained in different phases, depending on the employed synthesis method. Whereas bulk amorphous phase is generally considered to have negligible photocatalytic and antibacterial activity, recent research works pointed out the importance of the presence of an amorphous layer to boost the photocatalytic performance of TiO_2 [22]. Hydrogenated TiO_2 has attracted attention due to its optical absorption and high activity [23]. Unfortunately, the proposed synthesis method requires high pressure of hydrogen (up to 20 bar) and long annealing treatments (up to 15 days) [23]. As already mentioned, photoactivity can be ready to improved with metal grafting. Indeed, when in contact with small metal cluster, the charge separation and transfer process are faster and thermodynamically favoured [2, 59].

Recently, we proposed an alternative, industrially compatible, scalable and environmental friendly technique such as pulsed laser ablation in liquid (PLAL) for the synthesis of TiO_2 NPs in solution [58, 60]. In this work, we synthetized amorphous TiO_2 NPs characterized by a high degree of hydrogenation and high photocatalytic and antibacterial activity.

5.1. TiO_2 NPs obtained via laser ablation

The experimental details of the synthesis can be found in [58]. In **Figure 19**, representative TEM and SEM images of the TiO_2 NPs are reported. According to the electron microscopy, the particles resulted amorphous with a broad distribution in size (typical of the PLAL methodology).

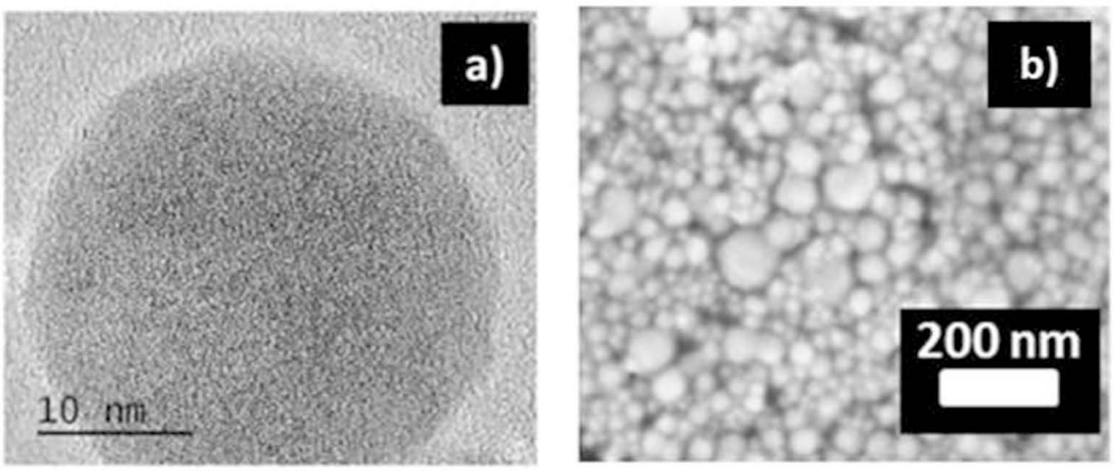

Figure 19. TEM (a) and SEM (b) images of LA-NPs. Reprinted with permission from Zimbone et al. [58]. Copyright ©2015, Elsevier.

This was further confirmed by the Raman analysis showing the characteristic convolution of peaks of the amorphous phase. In **Figure 20**, the Raman spectrum of LA-NPs is reported in comparison with the spectra of amorphous and crystalline (anatase or rutile) TiO_2.

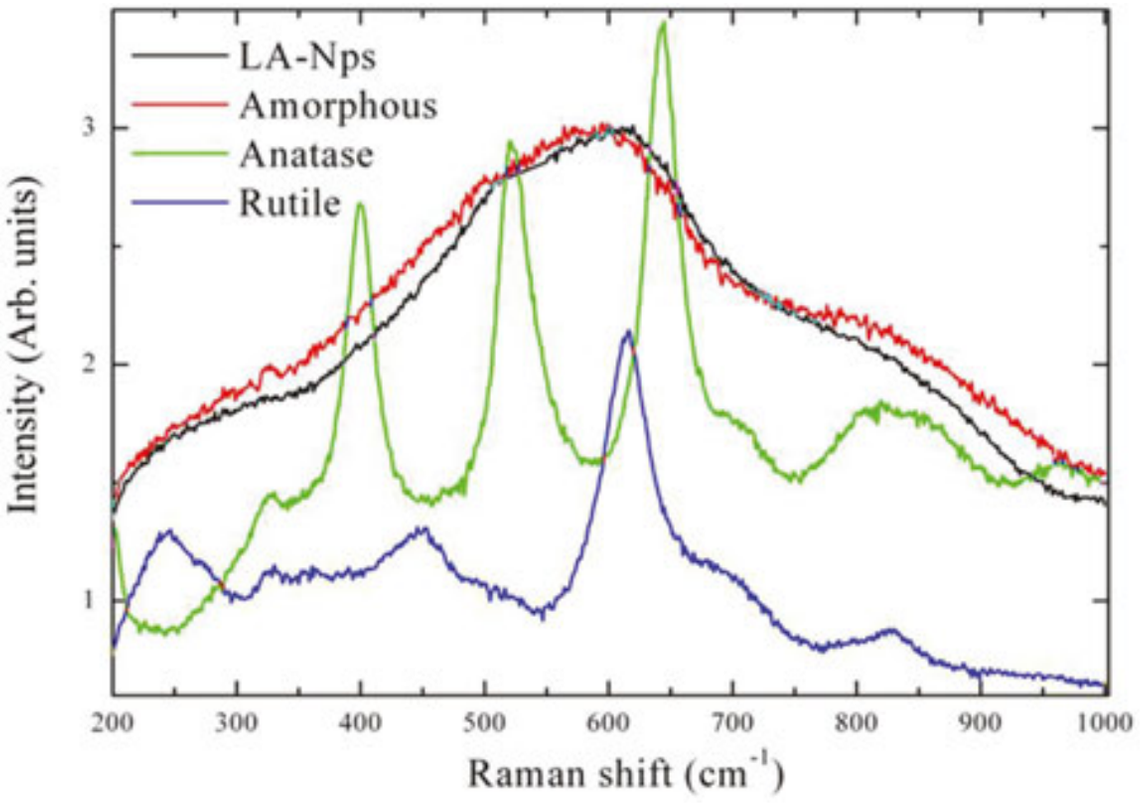

Figure 20. Raman response of LA-NPs compared with that of amorphous, rutile and anatase TiO_2 samples. Reprinted with permission from Zimbone et al. [60]. Copyright ©2016, Elsevier.

http://dx.doi.org/10.5772/62620

It is worth noting that the presence of hydroxyl groups in the TiO_2 NPs obtained via laser ablation (LA-NPs) has been evidenced by FTIR spectroscopy measurements. In **Figure 21**, the FTIR spectra of LA-NPs were compared with that of commercial TiO_2 NPs (C-NPs).

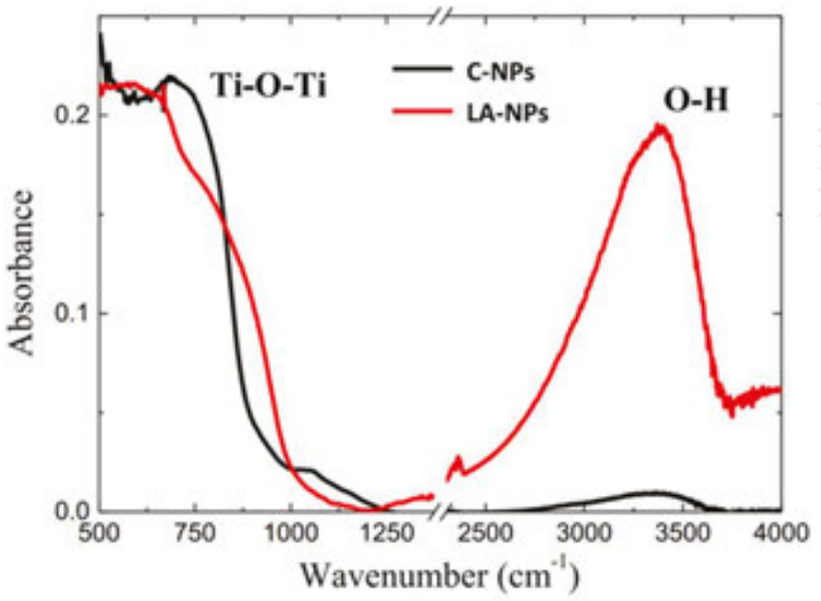

Figure 21. FTIR spectra of crystalline TiO_2 (C-NPs), and laser ablated nanoparticles (LA-NPs). Ti–O–Ti vibration and O–H stretching bands are referred in the Figure. Reprinted with permission from Zimbone et al. [60]. Copyright ©2016, Elsevier.

Hydrogen is identified by OH stretching at about 3400 cm^{-1} in FTIR spectra, as previously reported by Johnson et al. [61]. In the spectral range sampled in **Figure 21**, we clearly observe the typical absorption of TiO_2 in the 500–1000 cm^{-1} range and a strong absorption at 3000–3500 cm^{-1} due to the hydroxyl vibration. The amount of hydroxyl groups is directly related to the amount of hydrogen in or on the NPs surface [61]. In order to compare the amount of OH in LA-NPs and C-NPs, we can normalize the spectra to the TiO_2 signal in both samples. The number of hydroxyl groups in LA-NPs is found to be about one order of magnitude greater than the crystalline samples. We can state that pulsed laser ablation in water resulted in the formation of nm-sized hydrogenated TiO_2 NPs.

As reported in [58], photocatalytic activity of LA-NPs was found to be comparable to commercial crystalline NPs, while the antibacterial activity was found to be higher. These results are interpreted in terms of disorder and hydrogen inclusion in the structure of TiO_2 NPs. Interestingly, the mixture of LA-NPs with metal (Ag) NPs has been demonstrated to further improve their photocatalytic efficiency, as discussed in the next paragraph.

5.2. Ag/TiO_2 mixture

The synthesis of silver NPs (Ag-NPs) was performed by the PLAL method [55]. In **Figure 22** is shown a SEM image of the Ag-NPs. The particles appear spherical and have an average diameter of 25 ± 1 nm. From XRD, the presence of metallic Ag is confirmed.

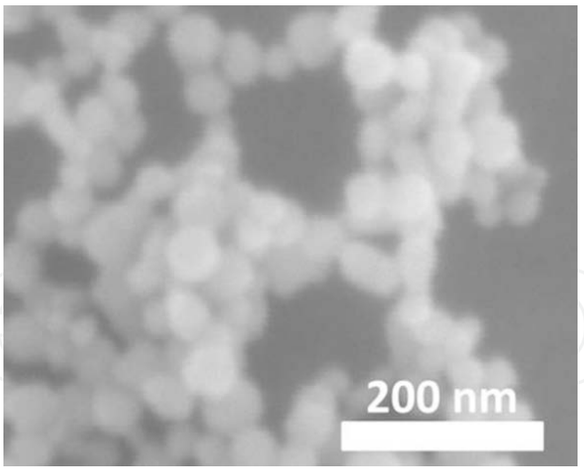

Figure 22. High magnification SEM image of laser ablated Ag nanoparticles.

In order to evaluate the effect of the Ag NPs on the photoactivity of LA-NPs, we performed MB discoloration tests [57] with a mixture of Ag-NPs and TiO_2 NPs obtained via laser ablation. We compared the resulting photocatalytic behaviour with LA-NPs without silver. In **Figure 23** are shown the absorbance spectra of MB solution in contact with LA-NPs (**Figure 23** left) and Ag–TiO_2 mixture (**Figure 23** right) versus time of irradiation. Note that in the presence of the Ag-NPs, the concentration of MB has decreased more than in the case of bare TiO_2.

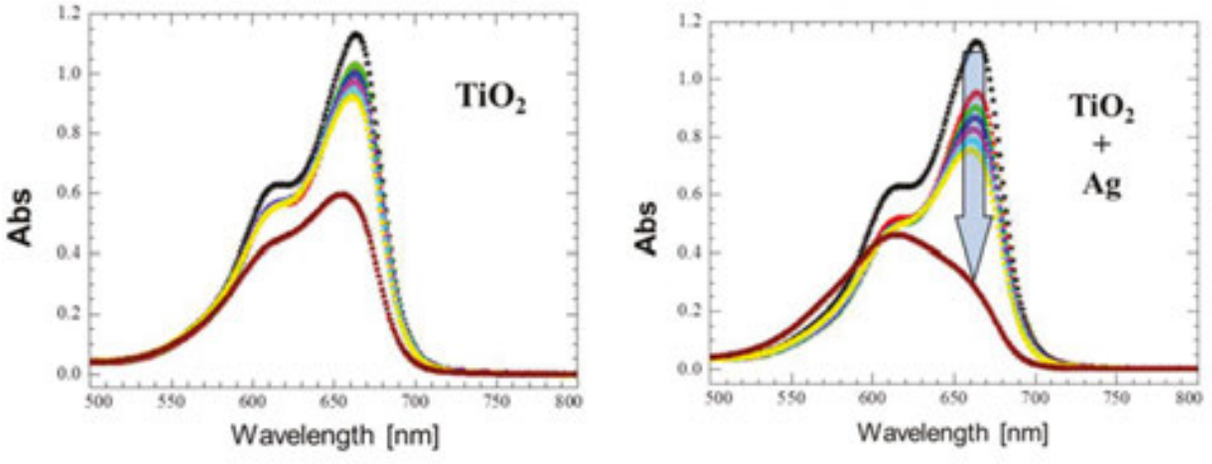

Figure 23. Absorbance of the MB solution in contact with LA-NPs (left) or a mixture of Ag and TiO_2 nanoparticles obtained by laser ablation (right) versus time.

The difference in the efficiency results more evident from **Figure 24**, where the normalized absorbance at 664 nm versus time for the two samples is reported. Note that this normalized value corresponds to the concentration of MB in solution according to $\frac{C}{C_0} = \frac{A}{A_0}$. The Ag–$TiO_2$ mixture shows clearly a better photocatalytic performance. Such enhancement is ascribable to the effect of the contact between Ag-NPs and TiO_2 LA-NPs. Indeed, the presence of a metal–

http://dx.doi.org/10.5772/62620

TiO_2 contact can effectively enhance the charge separation at the surface of NPs, thus increasing the carrier lifetime and the photocatalytic efficiency [6, 37].

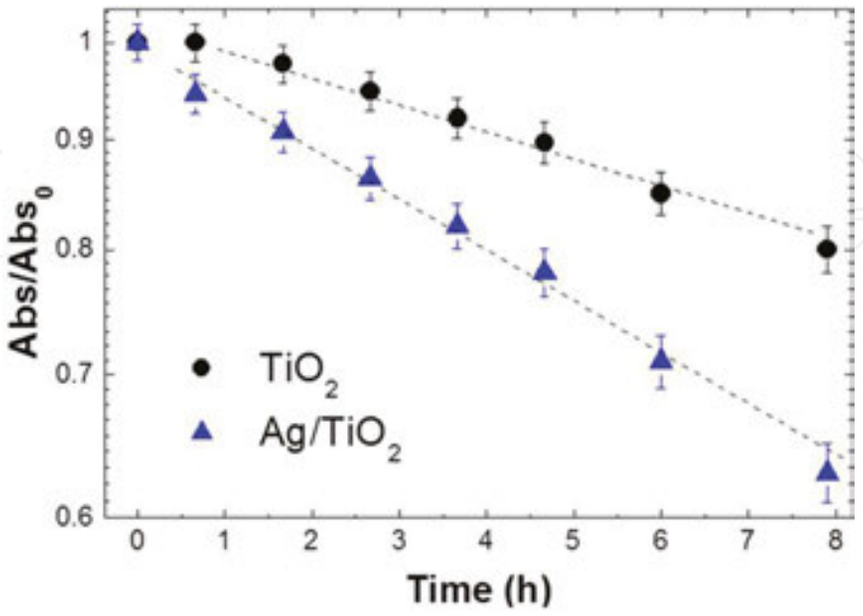

Figure 24. Normalized absorbance of the MB solution at the wavelength of 664 nm in the case of LA-NPs (black circles) and Ag–TiO_2 mixture (blue triangles) versus time.

5.3. Summary

We proposed TiO_2 NPs synthesis via PLAL as novel, environmental friendly, industrially scalable process in view of water purification strategies. Laser-ablated NPs (LA-NPs) have been found in highly disordered phase and with a high hydrogen content. Despite the amorphous phase, LA-NPs showed a photocatalytic activity similar to crystalline commercial powder and a higher antibacterial activity. This unexpected result has been explained taking into account the effects of disorder and hydrogen inclusion in the structure of TiO_2 NPs. The mixture of LA-NPs with Ag NPs obtained via laser ablation has been demonstrated to further improve the photocatalytic efficiency of TiO_2, thanks to an enhanced charge separation mechanism.

6. Conclusions

In the work presented in this chapter, two case studies have been presented: optical engineering of multilayered metal–TiO_2 thin films and TiO_2 NPs obtained via laser ablation.

In the thin film approach, we studied composite films of Ag NPs and TiO_2 for plasmon-enhanced photocatalysis. Using thermal dewetting or low-energy ion beam synthesis, metal NPs have been located at well-defined depth below the surface of a TiO_2 layer. We demon-

strated that the plasmonic effect can be effectively improved using an antireflective multilayer. This allows increasing the photon capture in a desired spectral range and enhancing this capture in a very thin layer near the surface. Photocatalytic activity has been observed under visible irradiation in multilayer Ag/TiO_2 nanocomposite samples in which the preparation procedure and stacking sequence were accurately selected. Such an activity, occurring at irradiation energies below the absorption threshold of titania (gap) and thus not observable in the bare TiO_2 film, has been ascribed to the presence of plasmonic metal NPs in field enhancement conditions. Therefore, the importance of proper film thickness engineering in order to take simultaneously advantage of plasmon resonances and optical interference has been evidenced.

In the other approach, TiO_2 NPs have been synthetized by PLAL, a novel, industrially scalable and eco-friendly technique. The LA-NPs were found to be in amorphous phase. Nevertheless, they showed a photocatalytic activity comparable to that of crystalline commercial powder and a higher antibacterial activity. This unexpected result has been explained taking into account the effects of disorder and hydrogen inclusion in the structure of TiO_2 NPs. In fact, these characteristics are reported to be responsible for the presence of superficial charge traps, which help the scavenging of electrons and, thereby, improve photocatalytic reactions. Mixing TiO_2 LA-NPs with Ag NPs has been demonstrated to further increase the photocatalytic efficiency of TiO_2, thanks to an enhanced charge separation.

Author details

Giuseppe Cacciato[1,2*], Massimo Zimbone[2], Francesco Ruffino[1,2] and Maria Grazia Grimaldi[1,2]

*Address all correspondence to: giuseppe.cacciato@ct.infn.it

1 Department of Physics and Astronomy, University of Catania, Catania, Italy

2 CNR-IMM, Catania, Italy

References

[1] Hashimoto K., Irie H., Fujishima. A. TiO_2 photocatalysis: A historical overview and future prospects. Jpn. J. Appl. Phys. 2005;44:8269–8285.

[2] Fujishima A., Zhang X., Tryk D.A. TiO_2 photocatalysis and related surface phenomena. Surf. Sci. Rep. 2008;63:515–582.

[3] Chong M.N., Jin B., Chow C.W.K., Saint C. Recent developments in photocatalytic water treatment technology: a review. Water Res. 2010;44:2997–3027.

[4] Hoffmann M.R., Martin S.T., Choi W., Bahnemann D.W. Environmental applications of semiconductor photocatalysis. Chem. Rev. 1995;95:69–96.

[5] Linsebigler A.L., Lu G., Yates J.T.Jr. Photocatalysis on TiO_2 surfaces: Principles, mechanisms, and selected results. Chem. Rev. 1995;95:735–758.

[6] Linic S., Christopher P., Ingram D.B. Plasmonic-metal nanostructures for efficient conversion of solar to chemical energy. Nat. Mater. 2011;10:911–921.

[7] Fujishima A., Honda K. Photolysis-decomposition of water at the surface of an irradiated semiconductor. Nature 1972;238:37–38.

[8] Gerischer H. Electrochemical behavior of semiconductors under illumination. J. Electrochem. Soc. 1966;113:1174–1182.

[9] Teoh W.Y., Scott J.A., Amal R. Progress in heterogeneous photocatalysis: From classical radical chemistry to engineering nanomaterials and solar reactors. J. Phys. Chem. Lett. 2012;3(5):629–639.

[10] Derfus A.M., Chan W.C.W., Bhatia S.N. Probing the cytotoxicity of semiconductor quantum dots. Nano Lett. 2004;4(1):11–18.

[11] Hanaor D.A.H., Sorrell C.C. Review of the anatase to rutile phase transformation. J. Mater. Sci. 2011;46:855–874 .

[12] Ohno T., Sarukawa K., Tokieda K., Matsumura M. Morphology of a TiO_2 photocatalyst (Degussa, P-25) consisting of anatase and rutile crystalline phases. J. Catal. 2001;203:82–86.

[13] Luttrell T., Halpegamage S., Tao J., Kramer A., Sutter E., Batzill M. Why is anatase a better photocatalyst than rutile? Model studies on epitaxial TiO_2 films. Sci. Rep. 2014;4:4043. doi:10.1038/srep04043

[14] Scanlon D.O., Dunnill C.W., Buckeridge J., Shevlin S.A., Logsdail A.J., Woodley S.M., et al. Band alignment of rutile and anatase TiO_2. Nat. Mater. 2013;12:798–801.

[15] GopalN. O., Lo H.-H., Sheu S.-C., Ke S.-C. A potential site for trapping photogenerated holes on rutile TiO_2 surface as revealed by EPR spectroscopy: An avenue for enhancing photocatalytic activity. J. Am. Chem. Soc. 2010;132:10982–10983.

[16] Nakamura R., Imanishi A., Murakoshi K., Nakato Y. In Situ FTIR studies of primary intermediates of photocatalytic reactions on nanocrystalline TiO_2 films in contact with aqueous solutions. J. Am. Chem. Soc. 2003;123:7443–7450.

[17] Mattioli G., Filippone F., AmoreBonapasta A. Reaction intermediates in the photoreduction of oxygen molecules at the (101) TiO_2 (Anatase) surface. J. Am. Chem. Soc. 2006;128:13772–13780.

[18] Asahi R., Morikawa T., Ohwaki T., Aoki K., Taga Y. Visible-light photocatalysis in nitrogen-doped titanium oxides. Science 2001;293:269.

[19] Litter M.I. Heterogeneous photocatalysis: Transition metal ions in photocatalytic systems. Appl. Catal. B 1999;23:89–114.

[20] Khan S.U.M., Al-Shahry M., Ingler W.B. Efficient photochemical water splitting by a chemically modified n-TiO_2. Science 2002;297:2243.

[21] Robel I., Subramanian V., Kuno M., Kamat P.V. Quantum dot solar cells. harvesting light energy with CdSe nanocrystals molecularly linked to mesoscopic TiO_2 films. J. Am. Chem. Soc. 2006;128(7):2385–2393.

[22] Chen X., Liu L., Yu P.Y., Mao S.S. Increasing solar absorption for photocatalysis with black hydrogenated titanium dioxide nanocrystals. Science 2011;331:746.

[23] Chen X., Liu L., Huang F. Black titanium dioxide (TiO_2) nanomaterials. Chem. Soc. Rev. 2015;44:1861.

[24] Hou W., Cronin S.B. A review of surface plasmon resonance-enhanced photocatalysis. Adv. Funct. Mater. 2013;23:1612–1619.

[25] Maier S. A. Plasmonics: Fundamentals and applications. New York: Springer; 2007.

[26] Bohren C.F., Huffman D.R. Absorption of light by small particles. New York: Wiley; 1983.

[27] Kelly K.L., Coronado E., Zhao L.L., Schatz G.C. The optical properties of metal nanoparticles: the influence of size, shape, and dielectric environment. J. Phys. Chem. B 2003;107:668–677.

[28] Mock J.J., Barbic M., Smith D.R., Schultz D.A., Schultz S. Shape effects in plasmon resonance of individual colloidal silver nanoparticles. J. Chem. Phys. 2002;116:6755.

[29] Noguez C. Surface plasmons on metal nanoparticles: the influence of shape and physical environment. J. Phys. Chem. C 2007;111:3806–3819.

[30] Zimbone M., Messina E., Compagnini G., Fragalà M.E., Calcagno L. Resonant depolarized dynamic light scattering of silver nanoplatelets. J. Nanopart. Res. 2015;17:402.

[31] Catchpole K.R., Polman A. Plasmonic solar cells. Opt. Express 2008;16(26):21793.

[32] Pavaskar P., Hsu I.-K., Theiss J., Hung W.H., Cronin S.B. A microscopic study of strongly plasmonic Au and Ag island thin films. J. Appl. Phys. 2013;113:034302.

[33] Hao E., Schatz G. C. Electromagnetic fields around silver nanoparticles and dimers. J. Chem. Phys. 2004;120:357.

[34] Awazu K., Fujimaki M., Rockstuhl C., Tominaga J., Murakami H., Ohki Y., et al. A plasmonic photocatalyst consisting of silver nanoparticles embedded in titanium dioxide. J. Am. Chem. Soc. 2008;130:1676–1680.

[35] Standridge S.D., Schatz G.C., Hupp J.T.. Distance dependence of plasmon-enhanced photocurrent in dye-sensitized solar cells. J. Am. Chem. Soc. 2009;131:8407–8409.

[36] Chen K.-H., Pu Y.-C., Chang K.-D., Liang Y.-F., Liu C.-M., Yeh J.-W., et al. Ag-nanoparticle-decorated SiO_2 nanospheres exhibiting remarkable plasmon-mediated photocatalytic properties. J. Phys. Chem. C 2012;116:19039–19045.

[37] Zhang X., Chen Y.L., Liu R.S., Tsai D.P. Plasmonic photocatalysis. Rep. Prog. Phys. 2013;76:046401.

[38] Dahl M., Liu Y., Yin Y. Composite titanium dioxide nanomaterials. Chem. Rev. 2014; 114:9853–9889.

[39] Liu E., Kang L., Yang Y., Sun T., Hu X., Zhu C., et al. Plasmonic Ag deposited TiO_2 nano-sheet film for enhanced photocatalytic hydrogen production by water splitting. Nanotechnology 2014;25:165401.

[40] Cacciato G., Bayle M., Pugliara A., Bonafos C., Zimbone M., Privitera V., et al. Enhancing carrier generation in TiO_2 by a synergistic effect between plasmon resonance in Ag nanoparticles and optical interference . Nanoscale 2015;7:13468–13476.

[41] Novotny L., Hecht B. Principles of Nano-optics. Cambridge, UK: Cambridge University Press; 2006.

[42] Ingram D.B., Linic S. Water splitting on composite plasmonic-metal/semiconductor photoelectrodes: evidence for selective plasmon-induced formation of charge carriers near the semiconductor surface. J. Am. Chem. Soc. 2011;133:5202–5205.

[43] Liu Z., Hou W., Pavaskar P., Aykol M., Cronin S.B. Plasmon resonant enhancement of photocatalytic water splitting under visible illumination. Nano Lett. 2011;11:1111–1116.

[44] Govorov A.O., Zhang H., Demir H.V., Gun'ko Y.K. Photogeneration of hot plasmonic electrons with metal nanocrystals: Quantum description and potential applications. Nano Today 2014;9:85–101.

[45] Christopher P., Xin H., Linic S. Visible-light-enhanced catalytic oxidation reactions on plasmonic silver nanostructures. Nat. Chem. 2011;3:467–472.

[46] Bayle M., Benzo P., Combe N., Gatel C., Bonafos C., Benassayag G., et al. Experimental investigation of the vibrational density of states and electronic excitations in metallic nanocrystals. Phys. Rev. B 2014;89:195402.

[47] Carles R., Farcau C., Bonafos C., Benassayag G., Bayle M., Benzo P., et al. Three dimensional design of silver nanoparticle assemblies embedded in dielectrics for raman spectroscopy enhancement and dark-field imaging. ACS Nano 2011;5:8774–8782.

[48] Mooradian A., Wright G.B. Observation of the interaction of plasmons with longitudinal optical phonons in GaAs. Phys. Rev. Lett. 1966;16:999.

[49] Mlayah A., Carles R., Landa G., Bedel E., Muñoz-Yagüe A. Raman study of longitudinal optical phonon-plasmon coupling and disorder effects in heavily Be-doped GaAs. J. Appl. Phys. 1991;69:4064–4070.

[50] Reznik D., Cooper S.L., Klein M.V., Lee W.C., Ginsberg D.M., Maksimov A.A., et al. Plane-polarized Raman continuum in the insulating and superconducting layered cuprates. Phys. Rev. B 1993;48:7624.

[51] Baumard J.F., Gervais F. Plasmon and polar optical phonons in reduced rutile TiO_{2-x}. Phys. Rev. B 1977;15:2316.

[52] Gonzalez R.J., Zallen R., Berger H. Infrared reflectivity and lattice fundamentals in anatase TiO_2s. Phys. Rev. B 1997;55:7014.

[53] Grujić-Brojčin M., ŠćepanovićM., DohčevićMitrovićZ., PopovićZ.V. Infrared study of nonstoichiometric anatase TiO_2 nanopowders. Science of Sintering 2006;38:183.

[54] Cacciato G., Ruffino F., Zimbone M., Reitano R., Privitera V., Grimaldi M.G. Au thin films nano-structuration on polycrystalline anatase and rutile TiO_2 substrates towards photocatalytic applications. Mat. Sci. Semiconduct. Proc. 2016;42:40–44.

[55] Cacciato G. Metal-TiO_2 nanocomposites towards efficient solar-driven photocatalysis [PhD thesis]. Catania; 2016.

[56] Ruffino F., Grimaldi M.G. Controlled dewetting as fabrication and patterning strategy for metal nanostructures. Phys. Status Solidi A 2015;1–23. doi:10.1002/pssa.201431755

[57] Mills A., Hill C., Robertson P.K.J.. Overview of the current ISO tests for photocatalytic materials. J. Photochem. Photobiol. A 2012;237:7–23.

[58] Zimbone M., Buccheri M.A., Cacciato G., Sanz R., Rappazzo G., Boninelli S., et al. Photocatalytical and antibacterial activity of TiO_2 nanoparticles obtained by laser ablation in water. Applied Catalysis B: Environmental 2015;165:487–494.

[59] Liu M., Inde R., Nishikawa M., Qiu X., Atarashi D., Sakai E., et al. Enhanced photoactivity with nanocluster-grafted titanium dioxide photocatalysts. ACS Nano 2014;8(7): 7229–7238.

[60] Zimbone M., Cacciato G., Buccheri M.A., Sanz R., Piluso N., Reitano R., et al. Photocatalytical activity of amorphous hydrogenated TiO_2 obtained by pulsed laser ablation in liquid. Mat. Sci. Semiconduct. Proc. 2016;40:28.

[61] Johnson O.W., De Ford J., Shaner J.W. Experimental technique for the precise determination of H and D concentration in rutile (TiO_2). J. Appl. Phys. 1973;44:3008.